AJNR

MR Imaging Artifacts of the Axial Internal Anatomy of the Cervical Spinal Cord

Andrew J. Curtin, Donald W. Chakeres, Robert Bulas, Carl P. Boesel, Mark Finneran and Eric Flint

AJNR Am J Neuroradiol 1989, 10 (1) 19-26
http://www.ajnr.org/content/10/1/19

MR Imaging Artifacts of the Axial Internal Anatomy of the Cervical Spinal Cord

Andrew J. Curtin[1]
Donald W. Chakeres[1]
Robert Bulas[1]
Carl P. Boesel[2]
Mark Finneran[1]
Eric Flint[1]

Transverse scans of the spinal cord routinely demonstrate signal variations related to the internal anatomy of the cord that do not accurately conform to histologic cross sections. This study evaluates the MR appearance of the axial anatomy of the spinal cord and provides correlation to histologic sections as a means to understand this discordance so that disease can be recognized more readily. Short TR/TE spin-echo studies, cardiac-gated multiecho spin-echo studies, and gradient-refocused-echo studies of normal excised human spinal cords, a normal volunteer, and gelatin phantoms were obtained by using the same imaging parameters at 1.5 T. Imaging artifacts were further investigated by using both a 128 × 256 and 256 × 256 matrix with a varying phase-encoded axis. Histologic sections of the excised cords, which were stained for myelin, iron, and cell bodies (Nissl), were used for correlation to the images. We found that significant Fourier truncation and partial-volume imaging artifacts modulated the MR display of the cord. On short TR/TE images a ring of high signal at the periphery of the cord was due to a truncation artifact. The appearance of the central portions of the gray and white matter was affected variably by partial-volume averaging depending on the matrix size. White-matter tracts of the cord were always lower in signal than was the gray matter on all pulse sequences. This finding was not due to iron deposition or CSF motion artifacts. We suspect that this probably was related to dense, longitudinal organization of spinal tracts and resultant anisotropy of water molecule motion similar to that seen in the pyramidal tracts, tendons, and ligaments.

We recommend the use of a 128 × 256 matrix with two averages (four excitations) when obtaining axial scans of the spinal cord in living subjects. Although truncation artifacts diminish image quality, the quality is superior to that of images obtained with a 256 × 256 matrix, in which longer scanning times result in motion artifacts and reduced signal to noise.

Several high-resolution MR imaging studies of the spine have been reported that describe the appearance of the nerve roots, spinal cord, bones, and subarachnoid and epidural spaces [1–8]. This study addresses the normal appearance of the transverse (axial) anatomy of the cervical spinal cord on MR images. With improvement in image quality, owing primarily to surface-coil imaging, recognizable signal variations within the spinal cord are routinely visible. However, the MR appearance does not accurately or simply reflect the normal histologic anatomy. The signal-contrast relationships of the gray and white matter of the cord are different from those of the brain [9]. This study attempts to explain the discordance between the histologic and MR appearances in order to define the normal spinal cord so that disease can be recognized more easily.

Truncation artifacts seen on sagittal images of the cervical cord have already been described [6, 7]. We speculated that some of the findings on axial MR were due to similar technical variations, so a detailed study was undertaken of MR images obtained in cadaver spinal cords, phantoms, and a normal volunteer.

Materials and Methods

Normal fresh human cadaver spinal cords were excised at autopsy. Transverse sections of the formalin-fixed cervical cord were stained for myelin by using Weigert's method, for cell

This article appears in the January/February 1989 issue of *AJNR* and the April 1989 issue of *AJR*.

Received May 11, 1988; accepted after revision September 7, 1988.

[1] Department of Radiology, Division of Neuroradiology, Ohio State University College of Medicine, 410 W. 10th Ave., Columbus, OH 43210. Address reprint requests to A. J. Curtin.

[2] Department of Pathology, Division of Neuropathology, Ohio State University College of Medicine, Columbus, OH 43210.

***AJNR* 10:19–26, January/February 1989**
0195–6108/89/1001–0019

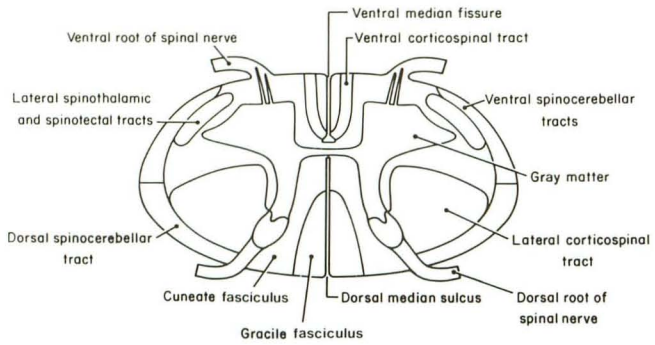

Fig. 1.—Axial anatomy of cord. Schematic drawing shows major spinal white-matter tracts and central gray matter.

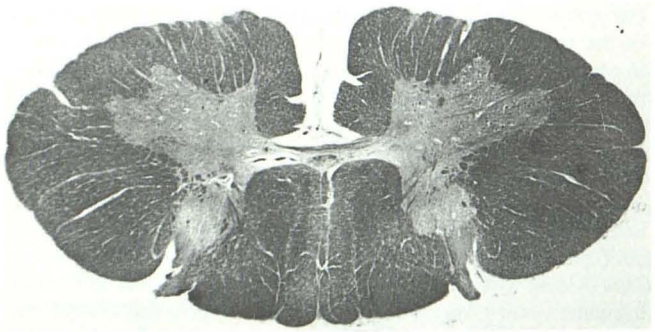

Fig. 2.—Myelin stain. Photomicrograph of normal human cervical cord. Transverse section is stained for myelin with Weigert's method. White-matter tracts stain more intensely than does butterfly-shaped central gray matter.

Fig. 3.—Photomicrograph of human cord at level similar to that of Fig. 2. White matter does not stain, but cell bodies in gray matter take up stain, seen as tiny, darker staining areas within gray matter. Very thin, dark rim at periphery is artifact of staining.

bodies by using a Nissl stain, and for ferric iron as per Gans [10] (Figs. 1–3).

All images were generated on a 1.5-T MR unit,* with a 10- by 28-cm license-plate-shaped receive-only surface coil. Slice thickness was 5 mm with a 1-mm gap between slices and one or two averages (two or four excitations). Fields of view were 16 and 20 cm. Both 128 × 256 and 256 × 256 matrices were used, varying the direction of the phase-encoded gradient. Imaging parameters included spin-echo images, 800/20/4 (TR/TE/excitations) (imaging times, 13 min 41 sec with a 256 × 256 matrix and 6 min 50 sec with a 128 × 256 matrix); gradient-refocused at a steady-state (GRASS) images [11], 1000/12/4, with a low flip angle of 22.5° (imaging times, 17 min 56 sec with a 256 × 256 matrix and 8 min 58 sec with a 128 × 256 matrix); as well as cardiac-gated spin-echo images, 2571/40,80/4 (imaging time, 22 min 1 sec with a 256 × 128 matrix).

Cylindrical, circular gelatin phantoms (1.4 and 2.5 cm in diameter), freshly excised cadaver spinal cords (Figs. 4C, 5C, and 6C), and a single normal volunteer (Figs. 4D, 5D, 6D, and 7C) were imaged with similar scanning parameters. The phantoms and excised cords were imaged both in air and in water baths (Figs. 4B, 5B, 6B, and 7B).

Images of the cadaver cords and the normal volunteer were analyzed and correlated with histologic sections, pixel diagrams, and phantom MR images.

Results

The transverse anatomy of the spinal cord has a central "butterfly" or an H configuration of gray matter (Fig. 1). The ventral collection of anterior horn cells is larger. A thin ventral commissure crosses the midline at the anterior third of the cord. The white-matter tracts are the major components of the cervical cord and surround this gray matter. Weigert's method stains the myelinated white-matter tracts (Fig. 2). The large dorsal columns of white matter form a triangle that appears as an upside-down V posterior to the central gray matter. The lateral and anterior tracts of white matter are composed predominantly of lateral cortical spinal tracts and envelop most of the remainder of the central gray matter. The ventral white-matter columns are much smaller than the posterior columns. The fissure is seen to be broader anteriorly than posteriorly.

Nissl's method stains the cell bodies of the central gray matter, which then appear as small areas of increased staining (Fig. 3). Because there is no peripheral gray matter there is no staining in this region. Iron stains, used to show normal deposits of physiologic iron in the brain, failed to show significant areas of ferric iron deposition (not shown).

Axial scans through the gelatin phantoms demonstrated an apparent ring of high signal at the surface of the gels (Figs. 4B, 5B, and 6B). With the 128 × 256 matrix, arcs or rings of alternating high and low signal were present within the phantom parallel to the surfaces along the phase and frequency axes only, producing variations in the signal (which one would expect to be homogeneous). These rings occurred in both the frequency- and phase-encoded directions but were thicker in the phase-encoded direction with 128 gradient steps. Switching the axis of the 128 phase-encoded gradient steps changed the direction of the thicker rings (Figs. 4B and 5B). The effect was more pronounced on the images of the smaller 1.4-cm-diameter gel. The artifact was significantly diminished with the 256 × 256 matrix size (Fig. 6B); however, a thin, bright-signal surface ring persisted. These ring patterns were present on both air and water bath (not shown) images of the phantoms, but were much more apparent on the air studies. In addition to producing apparent signal variations within the homogeneous gels, a geometric distortion also occurred,

* General Electric, Milwaukee.

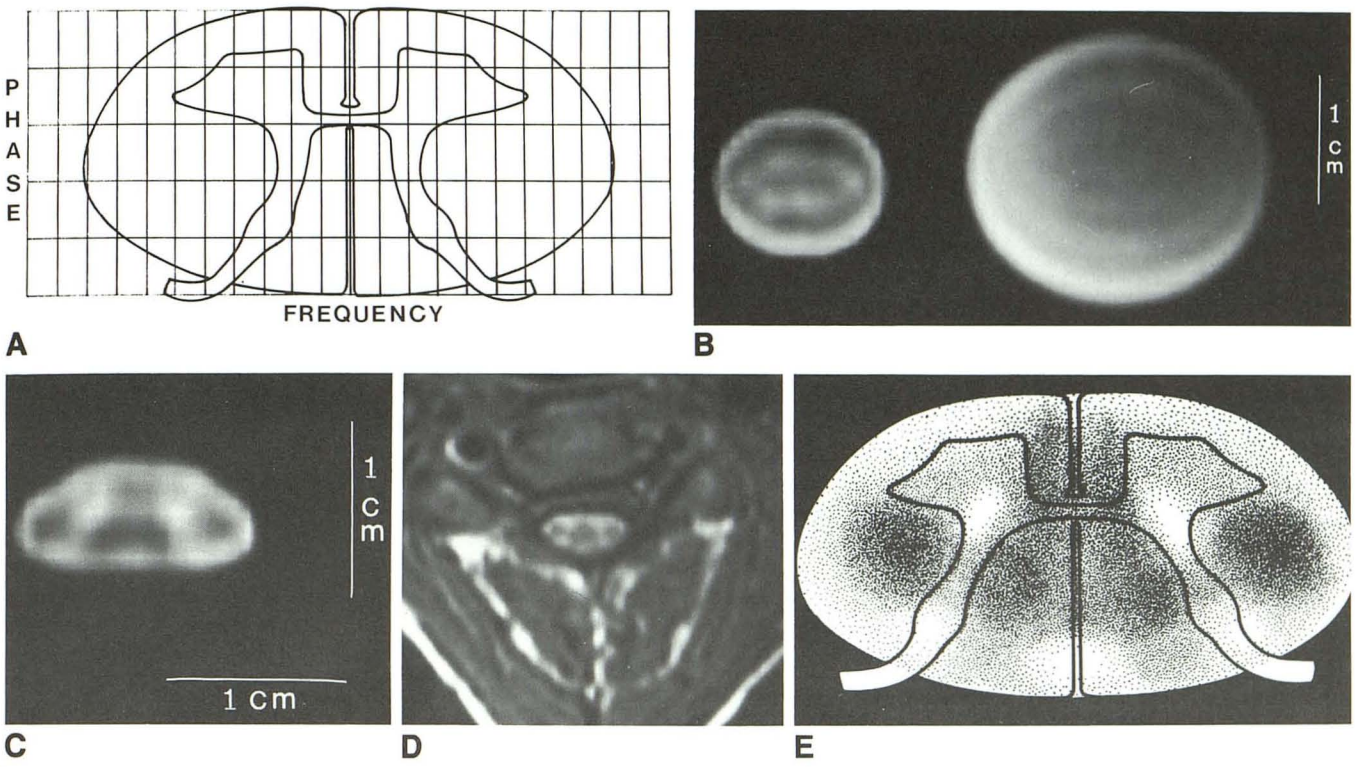

Fig. 4.—Pixel size and orientation.

***A*, Grid of rectangular boxes overlying transverse section of cord is drawn to scale approximating the number and size of pixels displaying the human cord when a 128 × 256 matrix and 16-cm field of view is used. Note that when 128 phase-encoded steps run anterior to posterior, only five pixels per row span cord.**

***B*, Gel phantom. Axial scan, 800/20, through cylindrical gelatin phantoms in air with 128 × 256 matrix and 128 in phase-encoded direction. Artifactual rings of high and low signal traverse internal structure of homogeneous phantom. Note high signal at periphery, which is thicker in phase-encoded direction. Geometric distortion of circular gel to more oval appearance is due to partial-volume effects.**

***C*, Excised cord. Axial scan of excised human cervical cord in air with parameters identical to those of gelatin phantom (*B*). High-signal rim that is thicker in phase-encoded direction surrounds two lateral circular areas of low signal overlying regions of corticospinal tracts. Butterfly-shaped area of high signal approximates gray matter. Central triangle of low signal approximates anterior and posterior columns.**

***D*, Human volunteer. Axial section of cervical spine, same parameters as *B* and *C*. Note that appearance is similar to that seen in excised cord (*C*).**

***E*, Location of gray-matter tracts with overlay drawing of approximate locations of high and low signal seen on short TR/TE images with 128 × 256 matrix.**

resulting in an oval shape on the transverse section (Figs. 4B and 5B), with the gel appearing more circular on the 256 × 256 matrix image (Fig. 6B).

The short TR/TE (800/20) MR images (Figs. 4C and 5C) of the excised cadaver cords surrounded by air demonstrated a high-signal ring at the periphery and two low-signal circular regions in the lateral cord substance. A paramidline lower-signal region was seen as a triangle that was broader posteriorly. These low-signal regions outlined two higher-signal regions that approximately, but not exactly, conformed to the central gray matter (Fig. 4E). The exact configuration of these findings varied, depending on the matrix size, voxel size, and direction of the phase-encoded gradient (Figs. 4C, 5C, and 6C). The findings were similar to those in the gelatin phantoms, in which the peripheral ring of high signal was thickest in the phase-encoded direction on the 128 × 256 matrix images. The appearance of the internal anatomy also changed with the phase-encoded axis, making the gray-matter structures appear to vary in configuration. Slight distortion of the external oval shape of the cord was present depending on the matrix size (Figs. 4C, 5C, and 6C). Visualization of the internal anatomy of excised human cord was best, and most accurately reflected the true anatomy, when two averages (four excitations) and a 256 × 256 matrix were used (Fig. 6C). Such high-quality definition of internal anatomy was not obtained in the living subjects with the 256 × 256 matrix/two averages technique (Fig. 6E).

Excised spinal cord imaged in a water bath with the spin-echo 800/20 technique produced images similar to those found for the cord imaged in air. The image showed the surrounding stationary water bath (not shown) as low signal with a high-signal ring present around the cord that was not as apparent as that seen in air.

The appearance of the excised cord surrounded by air with the GRASS technique appeared nearly identical to that of the short TR/TE sequences in air (Fig. 7A). However, when the cord was placed in a tube filled with water, the high-signal ring disappeared and the periphery was low signal (Fig. 7B). Spin-echo images of the excised cord, 2500/40, 80, were also obtained surrounded by air. The appearance of the internal anatomy on these long TR spin-echo images was similar to that on the other pulse sequences.

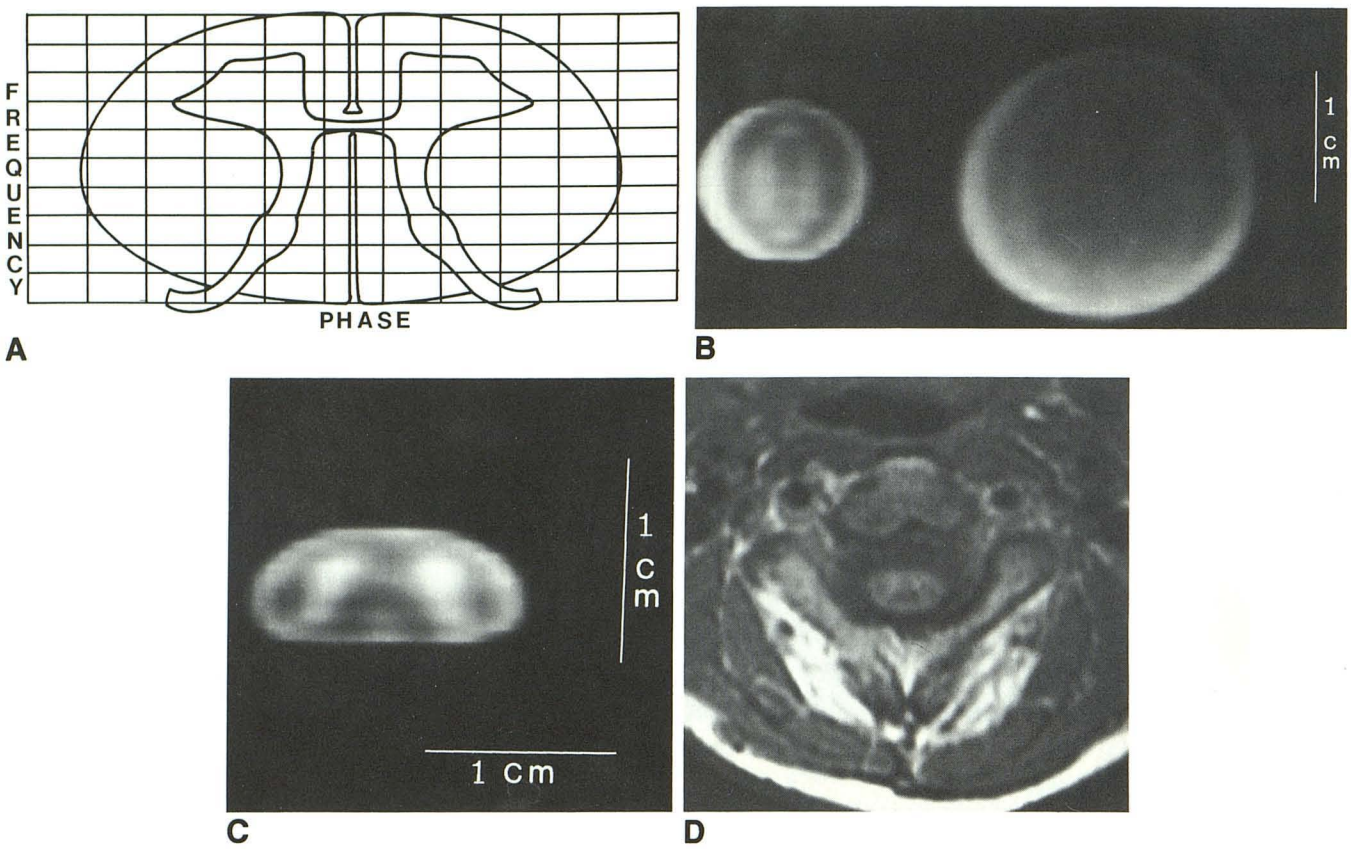

Fig. 5.—Voxel size and orientation, 128 × 256 matrix.

***A*, Pixel grid of 128 × 256 matrix, similar to Fig. 4A, but phase and frequency directions are reversed.**

***B*, Gel phantoms identical to those in Fig. 4B with same imaging parameters except phase and frequency directions switched. Note rim of high signal, thicker in phase-encoded direction, now runs from side to side.**

***C*, Excised cervical cord. Axial scan in air through same human cadaver at same level and with imaging parameters identical to those in Fig. 4C but with phase and frequency directions reversed. Lateral ovals of low signal have changed to more vertical oval orientation due to partial-volume effects, and entire cord has a more oval appearance. The same high-signal rim is apparent but is thicker from side to side in phase-encoded direction.**

***D*, Human volunteer. Axial scan again shows areas of high and low signal similar to that of excised cord.**

The 128 × 256 matrix volunteer studies with the short TR/TE spin-echo series, cardiac-gated, and non-cardiac-gated techniques produced images of the cord very similar to those of the excised cadaver cord (Figs. 4D and 5D). The use of a 256 × 256 matrix and only one average resulted in images of poor quality because of reduced signal-to-noise (Fig. 6D). With two averages (four excitations) and cardiac-gating, some of the internal anatomy of the cord was faintly visualized (Fig. 6E), but image quality did not have the resolution seen on the cadaver images. The volunteer studies with the GRASS technique and two averages (four excitations) produced images quite similar to those of the cadaver cord in a water bath (Figs. 7B and 7C), where the surrounding CSF was of high signal and the cord surface of low signal. Cardiac-gated spin-echo images, 2571/40,80 of the volunteer (Fig. 8) demonstrated an internal anatomy similar to that seen on the GRASS images, but the surface of the cord was seen less clearly. Nonetheless, the signal for the central gray and white matter remained constant, with the white matter always of lower signal than the gray matter on all pulse sequences.

As in the images of the gels, decreasing the voxel size by increasing the matrix to 256 × 256 or using smaller fields of view (16 cm) did not totally resolve the appearance of the rim of high signal at the periphery of the cord. The small-field-of-view, 256- by 256-matrix image quality of the volunteer studies was degraded by a reduced signal-to-noise ratio, causing poor visualization of the internal anatomy (Figs. 6D and 6E). To optimize visualization of the internal morphology it was necessary to decrease voxel size by using a larger matrix and smaller fields of view, but this required a larger number of averages. The images with the extended scanning times in the volunteer were compromised to some degree by voluntary and involuntary patient motion, so that the cord anatomy was not seen as well on most of the 256 × 256 images (Figs. 6D and 6E) as on the 128 × 256 images (Fig. 4D). Although internal cord anatomy was seen best in excised cord with 256 × 256 matrices and small fields of view, this could not be duplicated in living subjects despite gating and multiple averages.

Discussion

Many MR images of the cord in the axial plane do not correlate with histologic sections. On short TR/TE images, a

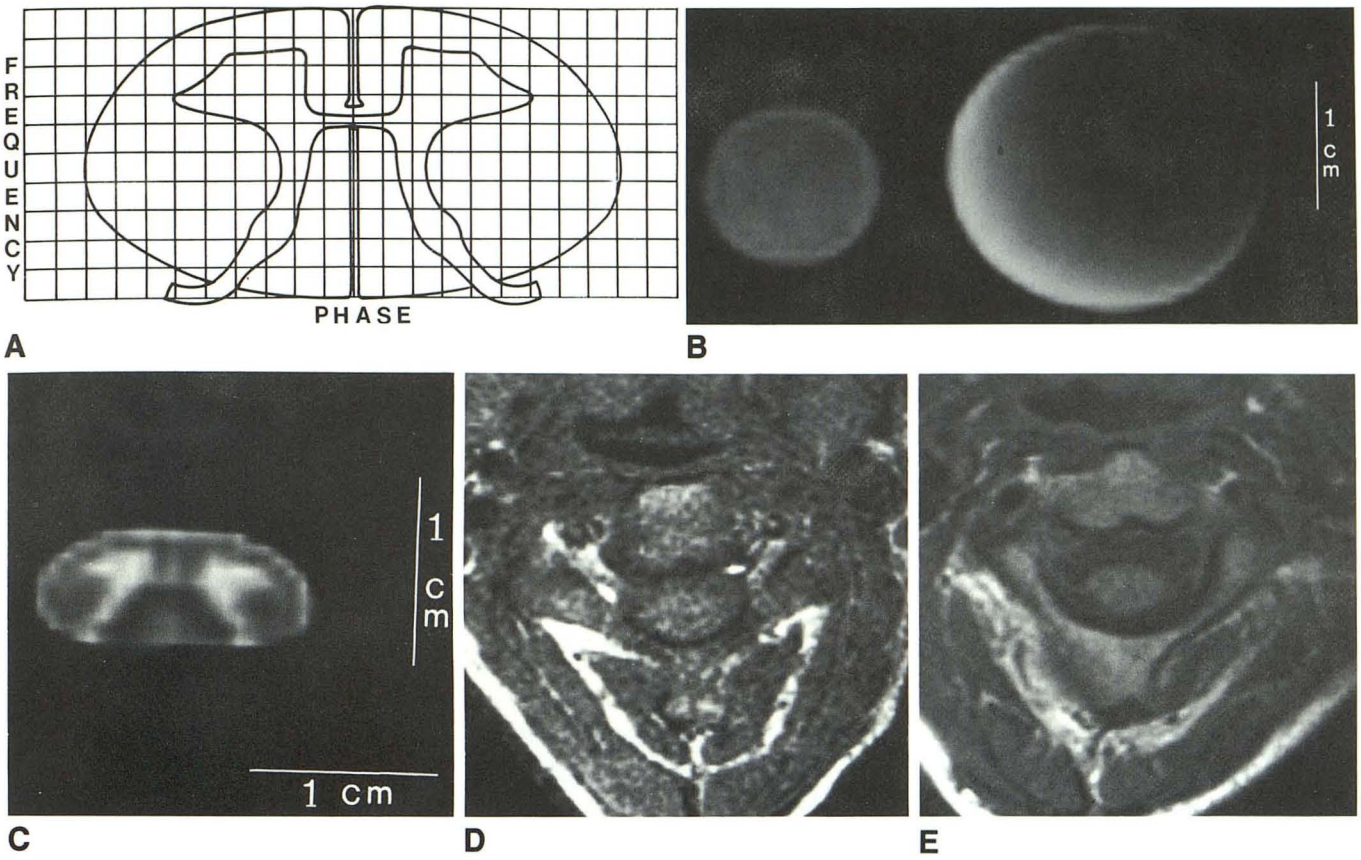

Fig. 6.—Voxel size and orientation, 256 × 256 matrix.

***A*, Grid overlies drawing of cord with 256 × 256 matrix and 16-cm field of view.**

***B*, Gel phantom. With 256 × 256 matrix, scan of same gelatin phantoms shows marked reduction in ring artifacts. Added data points of increased matrix size lessen effect of data truncation. Thinner peripheral rim of high-signal overshoot persists.**

***C*, Excised cord, same level as in Figs. 4C and 5C, in air. A truer representation of normal transverse anatomy as seen on histologic sections is now shown. Note that a thin rim of high signal persists at periphery.**

***D*, Human volunteer. Axial scan, 800/20, with only two excitations (one average) to maintain imaging time similar to that in Figs. 4 and 5. Image quality is severely diminished because of reduced signal-to-noise ratio of smaller voxel size and poor visualization of internal anatomy.**

***E*, Human volunteer with two averages (four excitations). Increased imaging time required cardiac gating for satisfactory results but still only faintly shows internal cord anatomy.**

high-signal ring is seen at the periphery of the cord that has a signal character similar to the central gray matter, but there is no corresponding gray matter at the surface of the cord (Figs. 1–3). Circular low-signal areas overlying regions of the lateral white-matter tracts are seen on MR, but there are no correlating anatomic structures on the histologic sections. The inhomogeneous appearance of the MR images obtained from scanning the gelatin phantoms also suggests that the MR appearance of the gray and white matter is modulated by superimposed artifacts, which may account for the inaccuracies.

Artifacts in MR imaging have been well described in the literature [12–14], including truncation artifacts on sagittal MR images of the cervical cord [6, 7]. Edge artifacts are generally ascribed to chemical shift, motion, and Fourier transformation truncation artifacts (Gibbs phenomenon). Chemical-shift artifacts are spatial errors in image location assignment that occur only in the frequency-encoded direction due to the slightly differing Larmor frequencies of different chemical species of protons. The superimposed artifacts seen in the phantom and spinal cord images occurred in both phase and frequency directions and do not appear to be due to chemical shift. Furthermore, there are no free triglyceride fats in the cord to produce chemical-shift artifacts.

Artifacts due to motion occur predominantly in the phase-encoded direction due to changes in the phase angle of moving protons across the gradients. In addition to simply blurring the images, motion artifacts can occur with sharp edges as "ghost images" or as image harmonics at periodic intervals along the phase-encoded direction that are dependent on TR and TE if there is a periodicity of the motion, as seen with CSF [15, 16]. In the cervical region, pulsatile CSF flow is a source of motion artifact [16, 17], but that does not explain artifacts seen in the cadaver or phantom studies. The cord had a similar appearance on gated and nongated examinations.

A third type of artifact is produced by limitations placed on sampling data for image reconstitution with the two-dimensional Fourier transformation (2DFT) technique [12–14]. The 2DFT techniques transform the frequency- and phase-en-

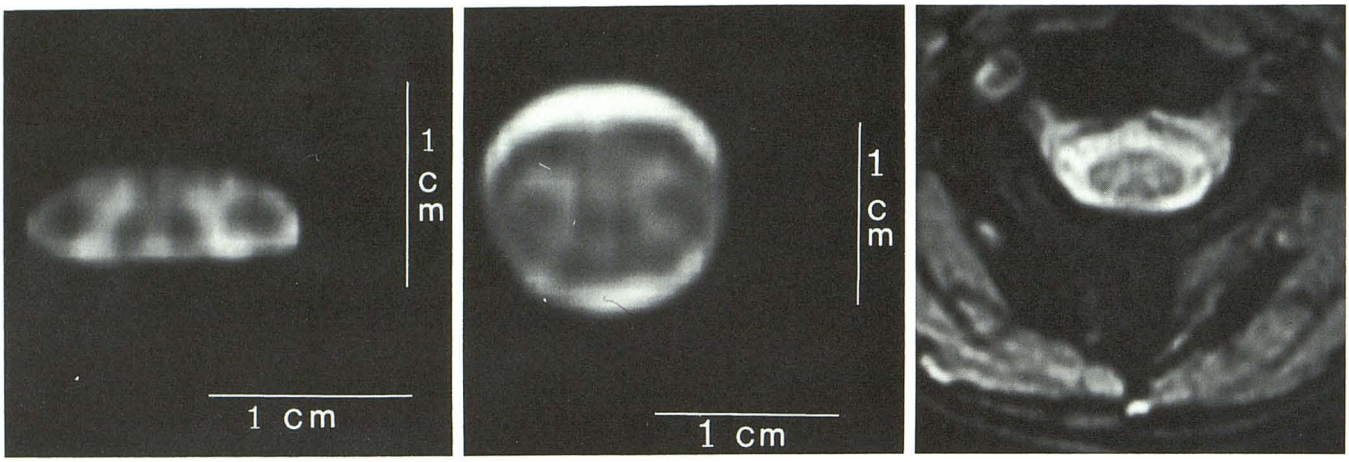

Fig. 7.—GRASS images.

***A*, Excised cord in air. Axial GRASS scan, 1000/12, of same level through human spinal cord with 22.5° flip angle and 128 × 256 matrix. Phase-encoded direction is anterior to posterior; image is very similar to Fig. 4C with short TR/TE sequence and high-signal overshoot artifact at periphery.**

***B*, Excised cord in water bath. When excised cord is imaged with GRASS technique in a water-filled test tube, higher signal from surrounding water results in boundary artifact that overshoots toward lower signal, giving darker rim to cord. Central gray matter appears as high signal similar to other pulse sequences.**

***C*, Human volunteer. Axial GRASS scan shows darker signal to edge of cord, as seen in cadaver cord within water bath.**

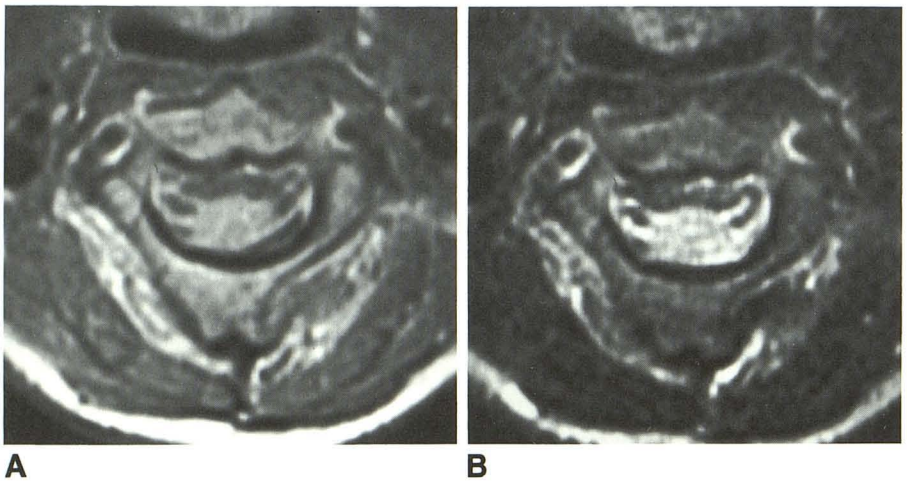

Fig. 8.—Gated spin-echo axial images, normal volunteer.

***A*, Cardiac gated images have much longer acquisition times, but anatomy is depicted less well. Effective TR is approximately 2500 msec with a TE of 40 msec and 128 × 256 matrix. CSF surrounding cord is isointense relative to gray matter of cord.**

***B*, Second echo of long TR sequence shows good visualization of nerve roots, but internal anatomy is not clear.**

coded information into an image. The image is a summation of a multitude of different sinusoidal waveforms. To accurately depict an object, particularly a complex one with abrupt, discrete edges, an infinite number of samples would need to be collected. However, this is not possible due to time constraints, so that data are truncated or approximated. An artifactual over- and undershoot occurs on both sides of the edge discontinuity. This artifact is called the Gibbs' or truncation artifact. In MR imaging, the results of this approximation are artifactual "ring"-like high and low signals parallel to an edge that occur on both sides of the discontinuity. Periodic overshoot and undershoot oscillations are dependent on the matrix size. The oscillations ripple across the image but decay rapidly. The size and periodicity of these striations are dependent on the pixel size in relation to the object and the matrix [6, 7]. 2DFT techniques truncate the data in both the phase and frequency directions, but the data truncation artifact is most evident in the phase-encoded direction, where data sampling uses only 128 gradient steps to save imaging time.

The edge "ringing" artifacts seen on the stationary gelatin phantom images occurred in both the phase and frequency directions and were the result of truncation artifacts. These artifacts were more severe in the smaller-diameter gel because fewer pixels spanned the section, thus accentuating the artifacts. An artifactual bright ring around the phantom was produced as the 2DFT approximation overshot the abrupt signal change from the signal void of air to the relatively higher signal of the gelatin. The use of long TR/TE or GRASS techniques to image the cord produced a high-signal CSF surrounding the cord so that the artifactual overshoot going from higher-signal CSF to relatively lower-signal cord resulted

in a lower-signal edge to the cord. The same type of truncation artifacts seem to modulate the images of the excised cadaver spinal cord as well as those of the normal volunteer.

Truncation artifacts can be reduced, although not eliminated, by increasing the matrix size (which increases the amount of data sampled), or by reducing the pixel size (field of view), which in effect reduces the size of the artifact in relation to the object. However, signal-to-noise considerations with smaller fields of view and a larger matrix size require extended imaging times [18], which may not be clinically practical. Even with short TR/TE images the multiple averages needed to obtain adequate signal-to-noise with a 256 × 256 matrix resulted in an image time of 13 min 41 sec for two averages (four excitations). Cardiac-gated long TR spin-echo images took 22 min 1 sec with two averages (four excitations) and a 128 × 256 matrix. Although our volunteer had a thin body habitus that maximized the signal and the proximity of the cord to the coil and was extremely cooperative, these protracted imaging times resulted in poorer quality than did shorter scanning times with the 256 × 128 matrix technique. We routinely use axial images with a 128 × 256 matrix and two averages (four excitations) for more consistent image quality in a reasonable amount of time (6 min 50 sec). Future development of better cervical spine surface coils may help resolve signal-to-noise considerations to provide greater resolution in a shorter scanning time.

Partial-volume averaging in digital imaging is also an important source of image distortion [19]. Partial-volume averaging occurs when the voxel is larger than the anatomic structure being imaged. Other adjacent structures are averaged, producing distortion of the image. Because the spinal cord is such a small structure, only a few pixels may span the entire cord (Figs. 4A and 5A). As few as five pixels compose the anterior to posterior cord on a 128 × 256 matrix with a 16-cm field of view (Fig. 4A). The internal appearance of the cord varied with a change in the phase-encoded axis because the pixels are larger than are portions of the cord gray matter, particularly the central commissure and dorsal horns. Geometric distortions to the size and normal oval shape of the cord also are attributable to partial-volume effects.

Previous studies evaluating the syrinxlike artifacts on sagittal images of the cord reported that axial scans obtained with GRASS techniques did not exclude the syrinxlike artifacts [7]. However, we did not find this artifact to be a problem and found that the use of two averages (four excitations) in GRASS-type imaging provides excellent demonstration of the internal anatomy. We suspect this artifact was avoided by using a 16-cm field of view.

The low signal of the white-matter columns in all pulse sequences is different from the appearance found in the brain. The brain white-matter tracts are higher in signal than is the gray matter on short TR/TE images and lower in signal on long TR/TE images. Iron staining of the cord failed to implicate iron deposition as a cause. Relaxation times of white and gray matter in the spinal cord remain an incompletely understood phenomenon. Accurate measurement of spinal cord relaxation times was not possible on our equipment because a region of interest small enough to exclude white matter from the sample area could not be obtained. Carvlin et al. [20] have reported initial experimental work measuring relaxation times that indicate spinal-cord gray matter has a longer T1, slightly shorter T2, and higher spin density compared with white matter. Yet their highly T1-weighted inversion-recovery images showed contradictory results of high signal to the spinal cord gray matter. They suspected that a higher spin density was the cause of this appearance, but concluded further quantitative studies would be necessary.

We speculate that the low signal of the dorsal and lateral white-matter columns may be due to the extreme longitudinal organization of ascending and descending myelinated axons in these columns, which may be thought of as analogous to the regular array of collagen fibers in a tendon or a ligament. As pointed out by Fullerton et al. [21], the low signal of a tendon is due primarily to the anisotropy of water molecule motion. Indeed, some other areas of white matter seem to show this phenomenon of low signal on all pulse sequences. The pyramidal tracts and medial lemniscus of the brainstem maintain a low signal on all pulse sequences, while the corpus callosum is bright on short TR/TE images. Both are white-matter structures and would be expected to have a similar signal, but the extreme organization of the longitudinal array of tracts in the brainstem most likely exhibits this same anisotropy of water molecule motion.

In summary, the MR appearance of the cervical cord on axial images is a representation of low-signal white-matter tracts and higher-signal gray matter modulated by truncation and partial-volume-averaging artifacts. In excised human spinal cord, the artifacts can be minimized and display of anatomy optimized by using a 256 × 256 matrix with at least two averages (four excitations). However, when imaging even the most cooperative volunteers in multiple averages, some patient motion and the reduced signal-to-noise aspects of a 256 × 256 matrix result in poorer image quality, such that the internal anatomy seen in the excised cord cannot be reproduced in the living subject. Although truncation artifacts are more pronounced with a 128 × 256 matrix, the smaller matrix is the most reliable and practical compromise for displaying the internal anatomy in patients. The use of two averages (four excitations) provides adequate delineation of the anatomy in most clinical situations with acquisition times under 7 min.

ACKNOWLEDGMENTS

We thank Melinda MaCalla, Cheryl Taylor, Linda Chakeres, Margaret O'Brien, and John Crouse for help in manuscript preparation.

REFERENCES

1. Flannigan BD, Lufkin RB, McGlade C, et al. MR imaging of the cervical spine: neurovascular anatomy. *AJNR* **1987**;8:27–32
2. Lee BCP, Deck MDF, Kneeland JB, Cahill PT. MR imaging of the craniocervical junction. *AJNR* **1985**;6:209–213
3. Norman D, Mills CM, Brant-Zawadzki M, Yeates A, Crooks LE, Kaufman L. Magnetic resonance imaging of the spinal cord and canal. *AJR* **1983**;141:1147–1152
4. Modic MT, Weinstein MA, Pavlicek W, Boumphrey F, Starnes D, Duchesneau PM. Magnetic resonance imaging of the cervical spine: technical and clinical observations. *AJR* **1983**;141:1129–1136

5. Hyman RA, Edwards JH, Vacirca SJ, Stein HL. 0.6 T MR imaging of the cervical spine: multislice and multiecho techniques. *AJNR* **1985**;6:229–236
6. Levy LM, Di Chiro G, Brooks RA, Dwyer AJ, Wener L, Frank J. Spinal cord artifacts from truncation errors during MR imaging. *Radiology* **1988**;166:479–483
7. Bronskill MJ, McVeigh ER, Kucharczyk W, Henkelman RM. Syrinx-like artifacts on MR images of the spinal cord. *Radiology* **1988**;166:485–488
8. Rubin JB, Enzmann DR. Optimizing conventional MR imaging of the spine. *Radiology* **1987**;163:777–783
9. Wehrli FW, MacFall JR, Glover GH, Haughton V, Johanson J. The dependance of nuclear magnetic resonance (NMR) image contrast on intrinsic and pulse sequence timing parameters. *Magn Reson Imaging* **1984**;2:3–16
10. Gans A. Iron in the brain. *Brain* **1923**;46:128–136
11. Enzmann DR, Rubin JB. Cervical spine: MR imaging with partial flip angle, gradient refocused pulse sequences. *Radiology* **1988**;166:467–472
12. Bellon EM, Haacke EM, Coleman PE, et al. MR artifacts: a review. *AJR* **1986**;147:1271–1281
13. Lufkin RB, Pusey E, Stark DD, Brown R, Leikind B, Hanafee WN. Boundary artifact due to truncation errors in MR imaging. *AJR* **1986**;147:1283–1287
14. Wood ML, Henkelman RM. Truncation artifacts in magnetic resonance imaging. *Magn Reson Med* **1985**;2:517–526
15. Rubin JB, Enzmann DR, Wright A. CSF-gated MR imaging of the spine: theory and clinical implementation. *Radiology* **1987**;163:784–792
16. Rubin JB, Enzmann DR. Harmonic modulation of proton MR precessional phase by pulsatile motion: origin of spinal CSF flow phenomena. *AJNR* **1987**;8:307–318
17. Rubin JB, Enzmann DR. Imaging of spinal CSF pulsation by 2DFT MR: significance during clinical imaging. *AJNR* **1987**;8:297–306
18. Bradley WG, Kortman KE, Crues JV. Central nervous system high-resolution magnetic resonance imaging: effect of increasing spatial resolution on resolving power. *Radiology* **1985**;156:93–98
19. Chakeres DW. Clinical significance of partial volume averaging of the temporal bone. *AJNR* **1984**;5:297–302
20. Carvlin M, Asato R, Hackney DB, Kasab E, Joseph PM. High resolution MRI of the spinal cord in humans and rats (abstr). *Magn Reson Imaging* **1987**;[Suppl 5]:56
21. Fullerton GD, Cameron IL, Ord VA. Orientation of tendons in the magnetic field and its effect on T2 relaxation times. *Radiology* **1985**;155:433–435